Original Article

THE METHOD OF VOLUMETRIC VISUALIZATION OF BONE DENSITY

Valerii Albertovich Dzhidzalov[1], Maryana Arturovna Bzhihova[2], Zaurbek Salambekovich Agaev[1], Gadzhimurat Magomedzapirovich Umarov[1], Bolatkhan Abdurashidovich Tovzerkhanov[1], Linda Ruslanbekovna Djamaldinova[2]*

[1]*Department of Therapy, Faculty of Dentistry of North Ossetian State University named after K.L. Khetagurov, Vladikavkaz, Republic of North Ossetia-Alania, Russia. bucky99@yandex.ru*
[2]*Department of Therapy, Faculty of Dentistry, North Ossetian State Medical Academy, Vladikavkaz, Republic of North Ossetia-Alania, Russia.*

https://doi.org/10.51847/2pnOTO5Qu6

ABSTRACT

The work aimed to optimize the technique of spatial digital analysis of bone density For the experiment, spiral computed tomography of the facial skeleton of 20 patients aged 10 to 22 years with maxillofacial pathology was performed. Spiral computed tomography technique (CT): the plane of the CT slice is parallel to the plane of the Frankfurt horizontal or the plane of the bite. The proposed technique makes it possible to visualize and, depending on the density, divide the bone tissue within each scan into a certain range of spectra, which makes it possible to better identify the zones with the highest and lowest density of bone tissue. The possibility of selecting a separate bone layer with a certain density range allows its reconstruction and tracing of its boundaries on a computer volumetric model. This technique can be successfully used in maxillofacial surgery, orthodontics, periodontics, and implantology to determine the condition of the bone tissue of the jaws to plan therapeutic measures.

Key words: Bones, X-ray density, Computed tomography, 3D visualization.

Introduction

To draw up a plan for both orthodontic and surgical treatment of bone pathologies of the dental system, criteria such as the patient's age, concomitant somatic diseases, localization of the pathological process, and the condition of the bone tissue in the affected area are increasingly taken into account . The latter is the most important in determining the type and scope of surgical intervention. Existing methods of X-ray studies allow us to assess the condition of the facial skeleton, both in two-plane projection (radiography) and in three-plane projection (spiral computed tomography), which produces a detailed high-resolution image of bone tissue on axial, frontal, and sagittal sections and in a volumetric SSD computer reconstruction [1-3]. This makes it possible to determine not only the exact localization and prevalence of the pathological process in the bone tissue but also to differentiate it by density [4, 5]. The software that currently exists allows marking bone tissue with a color index on the axial section according to the density gradient, which makes it possible to analyze bone density only within the axial plane [6-8]. This disadvantage does not provide a full-fledged stereoscopic spatial representation of the structure of bone tissue, and in some cases creates a false idea of the location of density zones due to the different angles of inclination of the scanning plane [9, 10]. If the latter error can be solved by observing the standard placement of the axial plane during scanning, then the spatial placement of bone density fields requires the development of additional techniques [11, 12]. The purpose of the study was to optimize the methodology of spatial digital analysis of bone density.

Materials and Methods

Archival data from spiral computed tomography (CT) studies of 20 patients aged 10 to 22 years with maxillofacial pathology were analyzed. To diagnose and plan treatment, spiral computed tomography of the facial skeleton was performed using the following technique: the CT plane of the slice is parallel to the plane of the Frankfurt horizontal or the plane of the bite **(Figure 1)**.

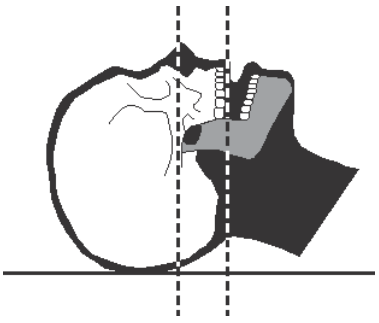

Figure 1. The layout of the axial slice plane during scanning

The computed tomography protocol for bone tissue identification was formed in accordance with another work [13]. The Gantry tilt angle was 0°. The reconstruction algorithm was billed as "bone" or "high resolution". The expansion of the matrix was 512 × 512. the thickness of the

slice is 1 mm, the rotation step is 1 mm, and the step during the reconstruction of the slice is 1 mm. The archived data was stored in DICOM format, and the analysis was carried out in the MATLAB R2006a software package and DICOM Works 1.3.5. more than 300 CT sections were analyzed, which were subjected to special processing in a computer program that included the darkening of soft tissues and marking of bone tissue **(Figure 2)**.

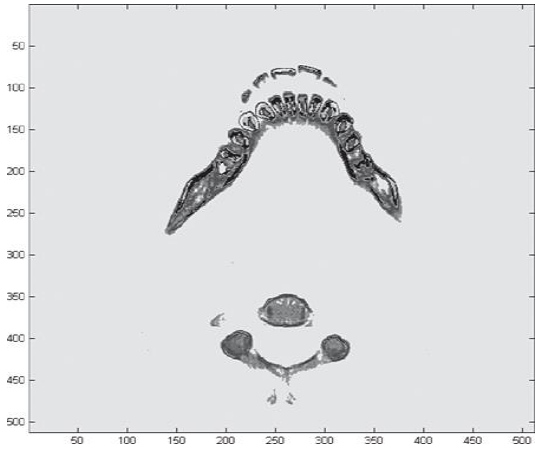

Figure 2. Image of axial section of jaw bone tissue.

Each range of bone density was assigned its color. Thus, the bone tissue was the largest in density and the teeth were marked in black, and the smallest in density was yellow. In the range between them, in ascending order, bone density was marked from green to blue in accordance with the color differentiation presented in the Guidelines for the diagnostic management of incidental solitary bone lesions on CT and MRI [14].

To map the spatial placement of bone density zones based on the MATLAB software platform, a mathematical algorithm has been developed for the degree of darkening of the image matrix with an upper and lower border, which makes it possible to isolate bone tissue of a certain density range and carry out their computer reconstruction independently of tissues of another density range. In this way, a solid-state computer reconstruction with ring-marked zones of four degrees of bone density was obtained. In the computer program DICOM Works 1.3.5, densitometric analysis of a series of axial slices was carried out to assign the units of Hounsfield (HU) to the corresponding color spectra.

Results and Discussion

To further determine the correspondence of bone density to certain color indicators, the image of the axial section of bone tissue is marked in the HSV color range. On the first series of axial sections, an image with the lowest density of bone tissue, marked with yellow and its shades, with a range of bone density of 400-162 HU was obtained **(Figure 3a)**.

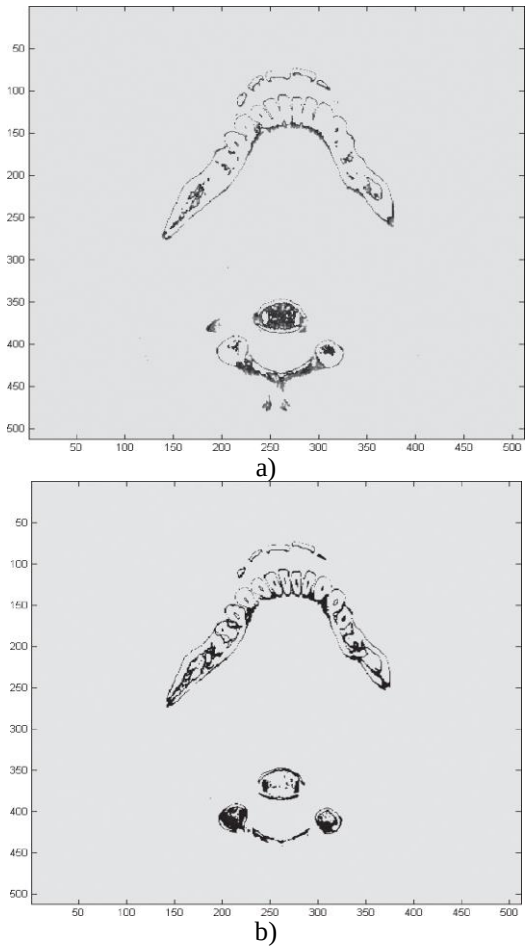

a)

b)

Figure 3. Axial sections encoded in HSV color format: with a bone density range of 400-162 HU (a), with a bone density range of 678-469 HU (b).

With the degree of dimming of the matrix of the second series of slices with an upper boundary of 100 units and lower boundary of 50 units in HSV mode, an image marked with a green color spectrum and its shades with a density range of 678-469 HU was obtained **(Figure 3b)**. With the degree of dimming of the matrix of the third series of axial sections with an upper boundary of 190 units and a lower boundary of 100 units in HSV mode, an image marked with a blue color spectrum and its shades with a bone density range of 1176-775 HU was obtained **(Figure 4a)**.

The selection of the last series of axial slices encoded by the HSV color format is not possible due to the fusion of the background and the bone marked with red with its shades of color, which significantly complicates visual analysis and makes further mathematical calculations not reliable **(Figure 4b)**. In this regard, the last range of bone density was encoded with the RGB (jet) color format. With the degree of dimming of the matrix of the fourth series of axial slices with an upper boundary of 280 units and a lower boundary of 190 units in RGB mode with excluded median and adaptive filtering, an image of bone

tissue marked with a spectrum of red with its shades of color was obtained **(Figure 5)**.

To obtain a color-marked volumetric image of bone tissue, SSD will reconstruct each color component that corresponds to a certain range of bone density **(Figure 6a)**. Combining SSD reconstruction of each color component, a volumetric reconstruction of the bones of the facial skeleton was obtained, marked in red, which corresponds to bone tissue with a density of 2107-1369 HU and yellow with a density of 400-162 HU **(Figure 6b)**.

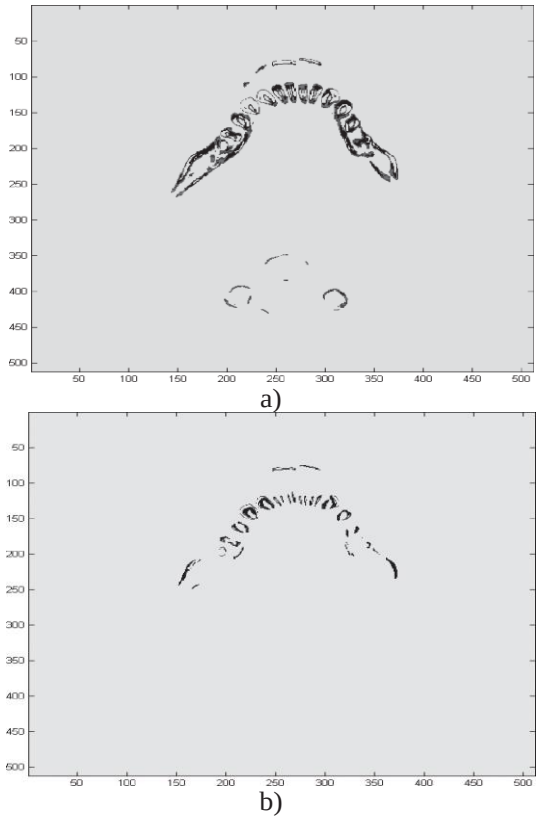

a)

b)

Figure 4. Axial sections encoded in HSV format: with a bone density range of 1176-775 HU (a), with a bone density range of 2107-1369 HU (b)

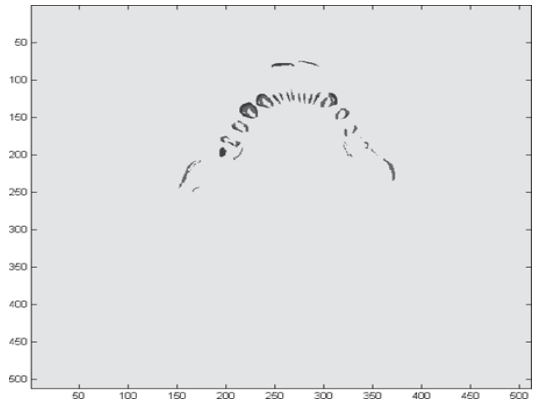

Figure 5. Axial slice encoded in RGB (jet) format with a bone density range of 2107-1369 HU

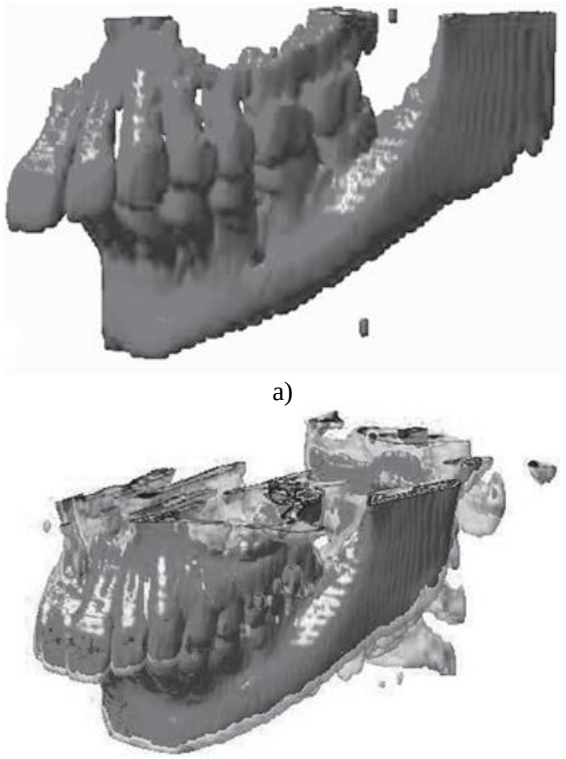

a)

b)

Figure 6. Computer SSD reconstruction of the jaw bone: with a density range of 2107-1369 HU (a); with a bone density range of 2107-1369 and 400-162 HU (b)

The analysis of the obtained image indicates the heterogeneity of the density of the bone tissue of the skull. Thus, bone tissue with a density index of 2107-1369 HU is localized mainly in the frontal region of the alveolar process of the upper jaw, the zygomatic-alveolar ridge forms the cortical layer of the angle, body, and chin of the lower jaw. This sector is also responsible for marking cement and dentin of teeth [14]. The visualization of these zones is clear, their boundaries are easily detected on the surface of the resulting reconstruction of the bones of the facial skeleton [15]. The analysis of computed tomography studies shows the correspondence between the indicators of densitometric analysis and images of axial sections decomposed into color spectra [16-19]. That is, each color corresponded to the limit of bone density, as evidenced by the dependence of digital indicators of bone density on the corresponding spectrum.

Conclusion

The proposed technique makes it possible to visualize and, depending on the density, divide the bone tissue within each scan into a certain range of color spectra, which makes it possible to better identify the zones with the highest and lowest density of bone tissue. The possibility of selecting a separate bone layer with a certain density range allows its reconstruction and tracing of its boundaries on a computer volumetric model. This technique can be successfully used

in maxillofacial surgery, orthodontics, periodontology, and implantology to determine the condition of the bone tissue of the jaws and to plan therapeutic measures.

Acknowledgments: None

Conflict of interest: None

Financial support: None

Ethics statement: The experiment was carried out under the guidelines of Ethical Comission of North Ossetian State Medical Academy, protocol #2/3 from 22.11.2022.

References

1. Roski F, Hammel J, Mei K, Baum T, Kirschke JS, Laugerette A, et al. Bone mineral density measurements derived from dual-layer spectral CT enable opportunistic screening for osteoporosis. Eur Radiol. 2019;29:6355-63. doi:10.1007/s00330-019-06263-z
2. Jin Z, Zhang F, Wang Y, Tian A, Zhang J, Chen M, et al. Single-photon emission computed tomography/computed tomography image-based radiomics for discriminating vertebral bone metastases from benign bone lesions in patients with tumors. Front Med. 2022;8:792581. doi:10.3389/fmed.2021.792581
3. Shevchenko YS, Plohova DP, Bulakhova IN, Mishvelov AE, Kubalova ME, Badriev GB, et al. Experience of carrying out magnetic resonance imaging with the use of specialized protocols and programs computer post-processing. Pharmacophore. 2020;11(2):77-81.
4. Mezhidov BS, Belyaeva AA, Kh SM, Bimarzaev S, Bektashev A, Shekhshebekova AM, et al. Prospects for creating 3D models of internal organs based on computer and magnetic resonance imaging images in emergency surgery and resuscitation. Pharmacophore. 2021;11(1):8-14. doi:10.51847/3TLcii4n42
5. Anderson AS, Sutherland ML, O'Donnell L, Hill EC, Hunt DR, Blackwell AD, et al. Do computed tomography findings agree with traditional osteological examination? The case of porous cranial lesions. Int J Paleopathol. 2021;33:209-19. doi:10.1016/j.ijpp.2021.04.008
6. Magomedova AS, Sheripovna DK, Kunkueva SA, Muskhanov MI, Ibragimov AK, Khazamova SO, et al. Application of a Simulation System Using Augmented Reality to Practice the Skills of Minimally Invasive Spine Surgery. J Pharm Res Int. 2021;33(42A):66-73. doi:10.9734/jpri/2021/v33i42A32385
7. Mishvelov AE, Ibragimov AK, Amaliev IT, Esuev AA, Remizov OV, Dzyuba MA, et al. Computer-assisted surgery: Virtual-and augmented-reality displays for navigation during planning and performing surgery on large joints. Pharmacophore. 2021;12(2):32-8. doi:10.51847/50jmUfdufI
8. Suleymanov TA, Kosinkova AM, Mishvelov AE, Povetkin SN, Simonov AN, Ziruk IV. Overview of the Holodoctor Software Package. Pharmacophore. 2020;11(2):65-72.
9. Tovlahanova TJ, Suleimanova MU, Dzaurova LH, Mezhieva MM, Murtazalieva BM, Durniyazov MN, et al. Study of the Effect of the Image Scanning Speed and the Type of Conductive Coating on the Quality of Sem-Micrographs of Oxide Nano Materials for Medical Use. Ann Med Health Sci Res. 2021;11(S3):60-4.
10. Valiukhov DP, Baklanov IS, Shtab EV, Shtab AV, Pigulev RV, Iliasov AS. Resonant-frequency properties of low-dimensional junction of semiconductor-metal-semiconductor and calculation methodology. InJournal of Physics: Conference Series 2019 Nov 1 (Vol. 1384, No. 1, p. 012002). IOP Publishing.
11. Maisigov JB, Kuznetsova GV, Magomedov AM, Adzhigova FZ, Magomedova AS, Burdukova SA, et al. Anthropometric Analysis of Digital Models of the Dentition Using 3D Technologies in Orthodontics. J Pharm Res Int. 2021;33(39B):101-5.
12. van Oosterom MN, van der Poel HG, Navab N, van de Velde CJH, van Leeuwen FWB. Computer-assisted surgery: virtual- and augmented-reality displays for navigation during urological interventions. Curr Opin Urol. 2018;28(2):205-13. doi:10.1097/MOU.0000000000000478
13. Nagdalian AA, Rzhepakovsky IV, Siddiqui SA, Piskov SI, Oboturova NP, Timchenko LD. Analysis of the content of mechanically separated poultry meat in sausage using computing microtomography. J Food Compost Anal. 2021;100:103918. doi:10.1016/j.jfca.2021.103918
14. Chang CY, Garner HW, Ahlawat S, Amini B, Bucknor MD, Flug JA, et al. Society of Skeletal Radiology–white paper. Guidelines for the diagnostic management of incidental solitary bone lesions on CT and MRI in adults: bone reporting and data system (Bone-RADS). Skeletal Radiol. 2022;51(9):1743-64. doi:10.1007/s00256-022-04022-8
15. Galabueva AI, Biragova AK, Kotsoyeva GA, Borukayeva ZK, Yesiev RK, Dzgoeva ZG, et al. Optimization of modern methods of treating chronic generalized periodontitis of mild severity. Pharmacophore. 2020;11(1):47-51.
16. Asgari I, Soltani S, Sadeghi SM. Effects of iron products on decay, tooth microhardness, and dental discoloration: a systematic review. Arch Pharm Pract. 2020;11(1):60-82.
17. Alamri AM, Alshammery HM, Almughamis MA, Alissa AS, Almadhi WH, Alsharif AM, et al. Dental Recession Aetiology, Classification and Management. Arch Pharm Pract. 2019;10(2):28-31.

18. Remizova AA, Dzgoeva MG, Tingaeva YI, Hubulov SA, Gutnov VM, Bitarov PA. Tissue dental status and features of periodontal microcirculation in patients with new covid-19 coronavirus infection. Pharmacophore. 2021;12(2):6-13. doi:10.51847/5JIbnUbHkT

19. Holland P, Quintana EM, Khezri R, Schoborg TA, Rusten TE. Computed tomography with segmentation and quantification of individual organs in a D. melanogaster tumor model. Sci Rep. 2022;12(1):2056. doi:10.1038/s41598-022-05991-5